Hindawi Publishing Corporation
Advances in Meteorology
Volume 2014, Article ID 963196, 10 pages
http://dx.doi.org/10.1155/2014/963196

Research Article

Climate Change Hotspots Identification in China through the CMIP5 Global Climate Model Ensemble

Huanghe Gu,[1,2] Zhongbo Yu,[1,3] Jigan Wang,[2] Qin Ju,[1] Chuanguo Yang,[1] and Chuanhao Fan[2]

[1] *State Key Laboratory of Hydrology-Water Resources and Hydraulic Engineering, Hohai University, Xikang Road 1, Nanjing 210098, China*
[2] *Business School, Hohai University, Xikang Road 1, Nanjing 210098, China*
[3] *Department of Geoscience, University of Nevada Las Vegas, Las Vegas, NV, USA*

Correspondence should be addressed to Zhongbo Yu; zyu@hhu.edu.cn

Received 15 February 2014; Revised 29 March 2014; Accepted 31 March 2014; Published 22 April 2014

Academic Editor: Eugene Rozanov

China is one of the countries vulnerable to adverse climate changes. The potential climate change hotspots in China throughout the 21st century are identified in this study by using a multimodel, multiscenario climate model ensemble that includes Phase Five of the Coupled Model Intercomparison Project (CMIP5) atmosphere-ocean general circulation models. Both high (RCP8.5) and low (RCP4.5) greenhouse gas emission trajectories are tested, and both the mean and extreme seasonal temperature and precipitation are considered in identifying regional climate change hotspots. Tarim basin and Tibetan Plateau in West China are identified as persistent regional climate change hotspots in both the RCP4.5 and RCP8.5 scenarios. The aggregate impacts of climate change increase throughout the 21st century and are more significant in RCP8.5 than in RCP4.5. Extreme hot event and mean temperature are two climate variables that greatly contribute to the hotspots calculation in all regions. The contribution of other climate variables exhibits a notable subregional variability. South China is identified as another hotspot based on the change of extreme dry event, especially in SON and DJF, which indicates that such event will frequently occur in the future. Our results can contribute to the designing of national and cross-national adaptation and mitigation policies.

1. Introduction

Global warming in the late 20th century has been primarily attributed to the anthropogenic greenhouse gas (GHG) emissions. According to the Fourth Assessment Report of the Intergovernmental Panel on Climate Change (IPCC), the average global warming is measured at 0.74°C (0.56°C to 0.92°C) over the last hundred years (1906 to 2005). The panel also predicts significant changes in the temperature and precipitation patterns by the end of the 21st century, which depends on the underlying GHG emission pathway [1]. The combined thermal and hydrological changes will increase the severity and frequency of droughts and floods, which will significantly affect water supply, agriculture, and human health [2–8]. Therefore, the manifestation of long-term global warming at regional scales must be identified even in highly uncertain terms [9–12]. For countries with large territory like China, it is important to assess local climate change impacts and to plan national policies response to global warming. In fact, observational studies reveal different climate trends in different areas of China [13–18]. Climate change hotspots that are most responsive to anthropogenic change must be identified to understand, prevent, and prepare for the impacts of climate change [19].

The hotspot is the region which is particularly vulnerable to the current or future climate change impacts and where the human security may be placed at risk. Identifying the potential impacts of climate change and showing the results in a map format can facilitate the communication and interpretation of such impacts [20]. The mapping of climate change hotspots has been widely practiced over the recent years [21–25]. Despite the lack of a standard practice

for quantitatively exploring these regions, climate change hotspots can be identified based on projected changes in temperature and precipitation. The Regional Climate Change Index (RCCI) of Giorgi is the first to determine climate change hotspots based on climate model outputs. RCCI is a comparative index that identifies the hotspot regions that will reveal the greatest relative changes in these variables [21]. Baettig et al. introduced the Climate Change Index (CCI) to measure the strength of future climate changes relative to the present natural variability [23]. Williams et al. [24] developed the standard Euclidean distance (SED) to measure the relative responses of different regions to GHG-induced global warming. Diffenbaugh et al. identified climate change hotspots in the United States using the SED and the squared cord distance dissimilarity coefficient (SCD), with both approaches yielding similar results [19]. Xu et al. used the RCCI to investigate the hotspots under 21st century global warming in East Asia [25]. The implementation of CMIP5 has paved the way for a new generation of global climate model simulations that can identify climate change hotspots and yield highly reliable projections [26–28].

The climate change hotspots in China that are identified based on the CMIP5 ensembles have not been sufficiently investigated. We focus our analysis on China for several reasons. First, China encompasses a large continental area with complex climatic conditions, fragile ecological environment, and frequent natural disasters and is one of the countries most vulnerable to adverse impact of climate change. Second, China has a massive population and a large and diverse economy that is at least partly dependent on climate, including a large fraction of the agricultural area [29, 30]. Third, as the largest developing country in the world, China plays a significant role in climate change negotiations because of the largest GHG emitters [31, 32] and because of the pressure to shoulder more responsibility for everything from curtailing carbon emissions to developing its economy, eradicating poverty, and improving people's livelihood.

This paper quantifies the hotspots in China through SED analysis. Section 2 describes the climate model data and the hotspot identification method. Section 3 discusses the results, and Section 4 presents the main conclusions and discussions.

2. Data and Methodology

2.1. Climate Model Data. CMIP5 multimodel experiments (obtained from the PCMDI website: http://pcmdi9.llnl.gov/esgf-web-fe/) are used in this study. 28 models in CMIP5 experiments from international laboratories that span a horizontal resolution of 1 degree to 4 degrees (Table 1) are used in this study. These models successfully capture the structure of temperature and precipitation over China [33, 34]. We quantify the climate change hotspots in the three periods of the CMIP5 RCP4.5 and RCP8.5 simulations, namely, 2010 to 2039, 2040 to 2069, and 2070 to 2099. These two simulations diverge dramatically over the 21st century, which can reach GHG concentrations of ~650 and >1370 ppm CO_2-e [35], respectively, and median global warming of 2.4°C and 4.9°C, respectively, above the preindustrial baseline by 2100 [36].

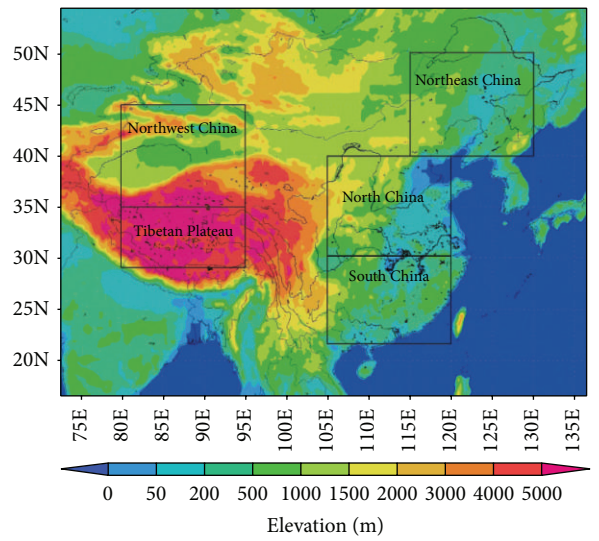

Figure 1: The elevation of study area and the five key analysis regions.

Following Giorgi [21] and Diffenbaugh et al. [19, 37], the analysis is performed after interpolating the output from each model to a common 1-degree geographical grid. Five subregions (Figure 1), namely, Northwest China, Tibetan Plateau, Northeast China, North China, and South China, are classified to compare the aggregate climate change of different climate zones.

2.2. Hotspot Identification. The SED of Williams et al. [24] and Diffenbaugh and Giorgi [37] is used to quantify the climate change hotspots in the CMIP5 ensemble. The SED synthesizes the changes in selected climate indicators to quantify the total change in a multidimensional climate space between the present and future periods. The SED has been widely used in previous studies to identify the potential climate change hotspots based on a large set of climate models. Diffenbaugh et al. [19, 37] used an improved version of SED to identify U.S. and global climate change hotspots. The total SED between the present and future periods at each grid point is calculated to measure the distance that is traveled in the multivariate climate space. The total SED is calculated as follows:

$$\mathrm{SED}_{\mathrm{total}} = \left(\sum_{v} \mathrm{SED}_{v} \right)^{1/2}. \tag{1}$$

We have

$$\mathrm{SED}_{v} = \frac{\left(x_{fv} - x_{pv} \right)^{2}}{\left\{ \max \left[\mathrm{abs} \left(x_{fv} - x_{pv} \right) \right]_{ij} \right\}^{2}}, \tag{2}$$

where x_{fv} denotes the value of variable v in the future period, x_{pv} denotes the value of variable v in the reference (present) period, and $\max [\mathrm{abs}(x_{fv} - x_{pv})]_{ij}$, which is used to normalize the metric, denotes the maximum land-grid-point

Table 1: Horizontal resolution (longitude × latitude in degree) of the 28 CMIP5 global climate models used.

	Model	Institution	Spatial resolution
1	BCC-CSM1.1	Beijing Climate Center (BCC), China	2.8125 × 2.8125
2	BCC-CSM1.1M	Beijing Climate Center (BCC), China	1.125 × 1.125
3	BNU-ESM	Beijing Normal University, China	2.8125 × 2.8125
4	CanESM2	Canadian Centre for Climate Modelling and Analysis, Canada	2.8125 × 2.8125
5	CMCC-CM	Canadian Centre for Climate Modelling and Analysis, Canada	0.75 × 0.75
6	CMCC-CMS	Canadian Centre for Climate Modelling and Analysis, Canada	1.875 × 1.875
7	CSIRO-Mk3-6-0	Australian Commonwealth Scientific and Industrial Research Organization (CSRIO), Australia	1.875 × 1.875
8	CSIRO-ACCESS1-0	CSRIO, Australia	1.875 × 1.2414
9	FIO-ESM	The First Institute of Oceanography, China	2.8125 × 2.8125
10	GFDL-ESM2M	Geophysical Fluid Dynamics Laboratory, USA	2.5 × 2
11	GISS-E2-H-CC	NASA Goddard Institute for Space Studies	2.5 × 2
12	GISS-E2-R-CC	NASA Goddard Institute for Space Studies	2.5 × 2
13	HadGEM2-AO	Met Office Hadley Centre, UK	1.875 × 1.2414
14	HadGEM2-ES	Met Office Hadley Centre, UK	1.875 × 1.2414
15	INM-CM4	Institute for Numerical Mathematics	2 × 1.5
16	IPSL-CM5A-LR	Institut Pierre-Simon Laplace, France	3.75 × 1.875
17	IPSL-CM5A-MR	Institut Pierre-Simon Laplace, France	2.5 × 1.2587
18	IPSL-CM5B-LR	Institut Pierre-Simon Laplace, France	3.75 × 1.875
19	MIROC5	AORI (Atmosphere and Ocean Research Institute), NIES (National Institute for Environmental Studies), JAMSTEC (Japan Agency for Marine-Earth Science and Technology), Japan	1.4063 × 1.4063
20	MIROC-ESM	AORI, NIES, JAMSTEC, Japan	2.8125 × 2.8125
21	MIROC-ESM-CHEM	AORI, NIES, JAMSTEC, Japan	2.8125 × 2.8125
22	MPI-ESM-LR	Max Planck Institute for Meteorology, Germany	1.875 × 1.875
23	MPI-ESM-MR	Max Planck Institute for Meteorology, Germany	1.875 × 1.875
24	MRI-CGCM3	Max Planck Institute for Meteorology, Germany	1.125 × 1.125
25	NCAR-CCSM4	National Center for Atmospheric Research (NCAR), USA	1.25 × 0.9375
26	NCAR-CESM1-BGC	NCAR, USA	1.25 × 0.9375
27	NCAR-CESM1-CAM5	NCAR, USA	1.25 × 0.9375
28	NorESM1-M	Norwegian Climate Centre, Norway	2.5 × 1.875

absolute value change in the climate indicator v over all land grid points ij in the future period (2070–2099) under RCP8.5 scenario. An area with a high SED_v score experiences more significant changes in variable v as compared to other areas with lower SED_v scores.

Seven indicators are considered in the analysis, namely, absolute change in mean 2 m temperature (T), fractional change in interannual standard deviation of de-trend 2 m temperature (T_{var}), fractional change in mean precipitation (P), fractional change in interannual coefficient of de-trend precipitation variation (P_{var}), frequency of occurrence of years above the baseline maximum seasonal surface air temperature (Hot), frequency of occurrence of years above the baseline maximum seasonal precipitation (Wet), and frequency of occurrence of years below the baseline minimum seasonal precipitation (Dry). The last three indicators represent extreme climate conditions that can severely affect human welfare and the environment. Each climate indicator is treated separately in each of the four seasons (DJF, MAM, JJA, and SON), which yields 28 climate dimensions. We calculate these 28 variable changes between the baseline (1970 to 1999) and future periods (2010 to 2039, 2040 to 2069, and 2070 to 2099) at each 1-degree grid point for the SED calculation. Temperature variability and precipitation variability are calculated as follows.

Temperature variability is

$$\Delta T_{\mathrm{var}} = \frac{\left(T_{\mathrm{SD,future}} - T_{\mathrm{SD,baseline}}\right)}{T_{\mathrm{SD,baseline}}}. \quad (3)$$

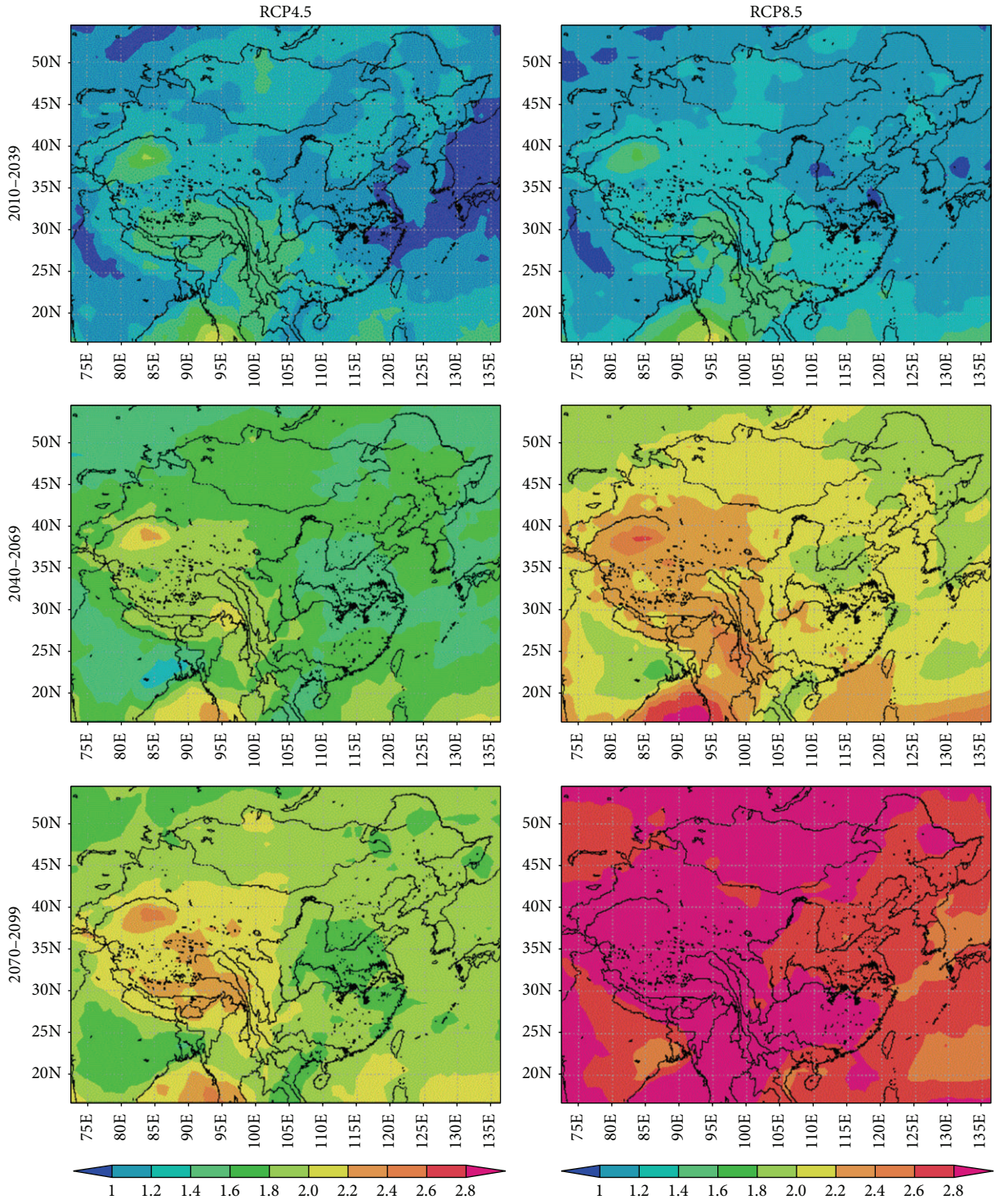

Figure 2: The relative aggregate climate change calculated using the standard Euclidean distance (SED) between the period from 1970 to 1999 and the RCP4.5 and RCP8.5 periods: 2010–2039, 2040–2069, and 2070–2099.

Precipitation variability is

$$\Delta P_{\text{var}} = \frac{\left[\left(P_{\text{SD,future}}/P_{\text{mean,future}}\right) - \left(P_{\text{SD,baseline}}/P_{\text{mean,baseline}}\right)\right]}{\left(P_{\text{SD,baseline}}/P_{\text{mean,baseline}}\right)}, \quad (4)$$

where SD denotes the standard deviation of the variable and future and baseline denote the future (2070 to 2099) and the baseline (1970 to 1999) periods, respectively.

The SED is a comparative index that compares climate change signals across regions. It provides a metric aggregation

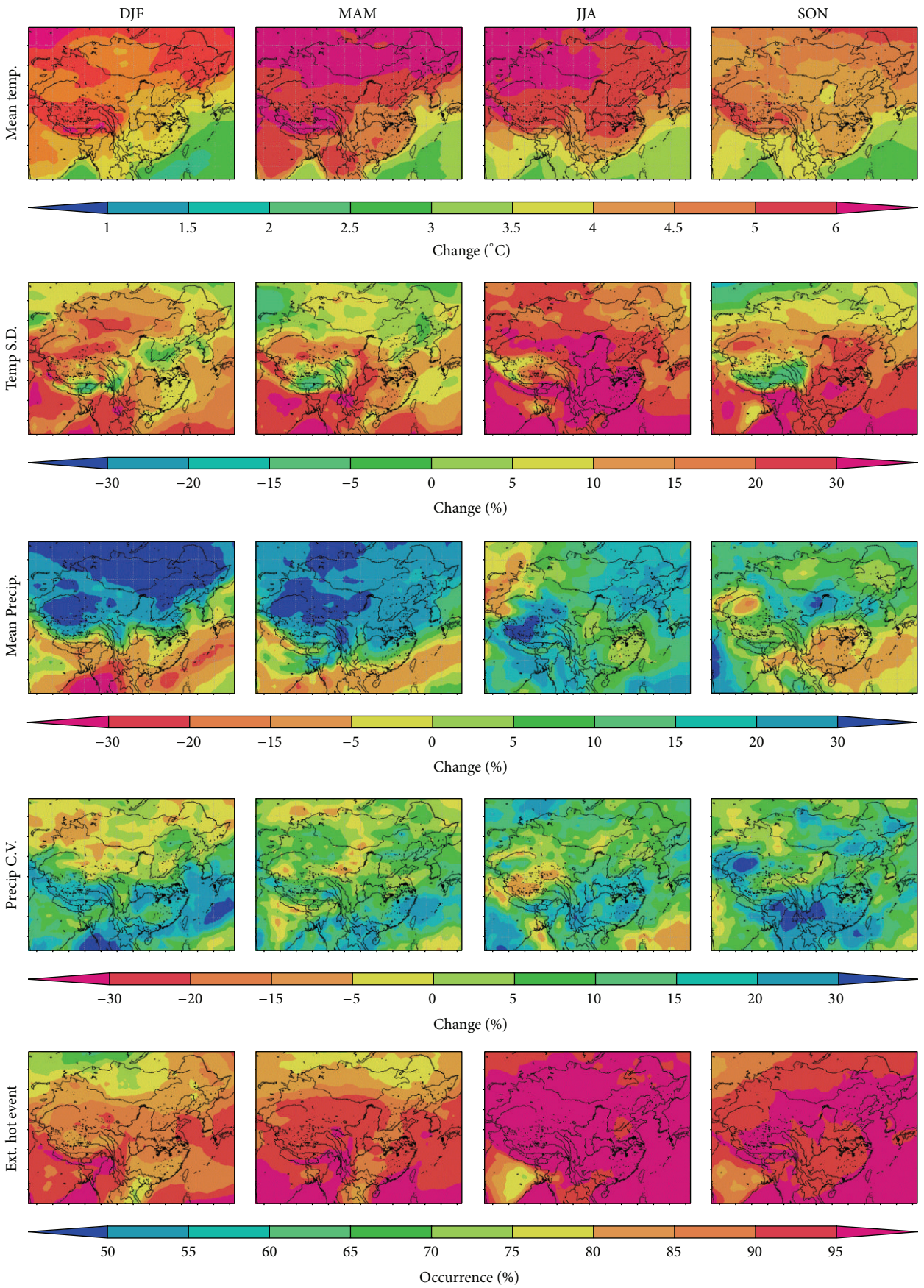

(a)

Figure 3: Continued.

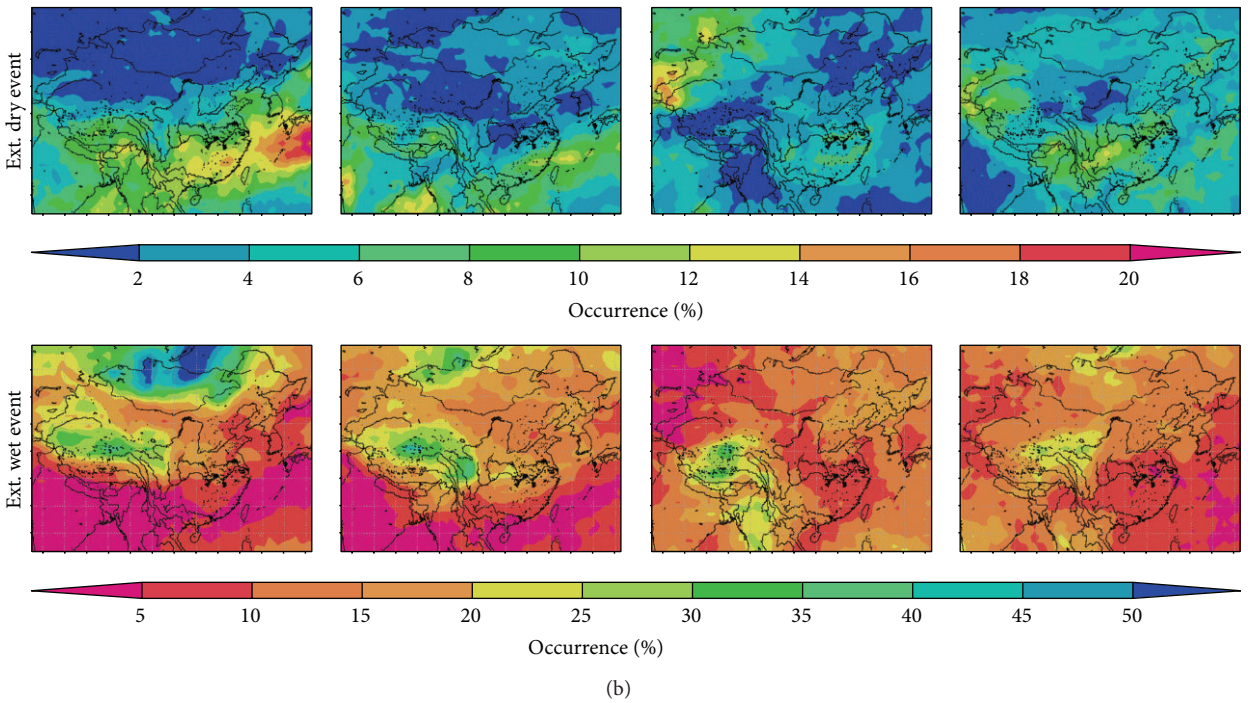

Figure 3: The change in each variable between the period from 1970 to 1999 and the period from 2070 to 2099.

of positive and negative changes in a number of climate variables of different scales and units. The regions with the strongest aggregate climate changes exhibit large relative changes in several climate indicators. However, the SED cannot be considered as an absolute indication of the signal magnitude which means that the small SED values are not necessarily an indication of a small magnitude of the climate change signal.

3. Results

Figure 2 shows the hotspot patterns for the three future time periods of RCP4.5 and RCP8.5. The relative aggregate climate change that is reflected by SED increases over time and across different scenarios because of its dependence on GHG emissions and concentrations. The dominant hotspot pattern in China, including Tarim Basin and south Tibetan Plateau, emerges in the early 21st century and exhibits relatively high aggregate climate change in all three periods of both forcing pathways. The other areas in China exhibit a relatively small yet increasing aggregate climate change throughout the 21st century. The relative aggregate climate change in RCP8.5 is more significant than that in RCP4.5, except for the average value in the period from 2010 to 2039, which shows similar changes because of the similar GHG concentrations in the two scenarios during this period [35]. The relative aggregate climate change of the two forcing pathways is fairly robust across different periods. The pattern of SED hotspots exhibits low sensitivity to time evolution and total concentration. Our metric also reveals that the North China Plain exhibits relatively small aggregate change to global warming.

Figure 3 shows the changes in the mean, variability, and extremes of seasonal temperature and precipitation between the period from 1970 to 1999 and the period from 2070 to 2099. The seasonal temperature in most parts of China will increase more than 3°C by the end of the 21st century, and the increase will exceed 4°C during MAM and JJA. The temperature variability in the south Tibetan Plateau will generally increase and slightly decrease during MAM and SON. The mean precipitation will increase in north China, while it will decrease in South China especially during DJF and SON. The precipitation variability in China will increase as a whole, increase significant in Tarim Basin and southwest China in SON, while decrease in Tibetan Plateau in JJA. The extreme hot event will significantly increase by the end of the 21st century, which is expected to cover more than 80% of the year. These events are hotter than their corresponding maximum seasonal temperature in the baseline period, especially during the JJA and SON. The change of extreme dry events is not obvious, except for the 10% increase in South China during DJF and SON. The extreme wet event will slightly increase in most parts of China, and there was an obvious increase in the Tibetan Plateau. The regions that exhibit the strongest aggregate climate changes also demonstrate large relative changes in several climate indicators. For example, in the period from 2070 to 2099, the Tibetan Plateau will exhibit relatively large changes in mean temperature during DJF and MAM, temperature variability and mean precipitation during DJF and JJA, precipitation variability during DFJ, extreme hot during MAM, and extreme wet during all seasons. The Tarim Basin will also exhibit relatively large changes in mean temperature during JJA; temperature variability in all seasons; mean precipitation during DJF, MAM, and JJA;

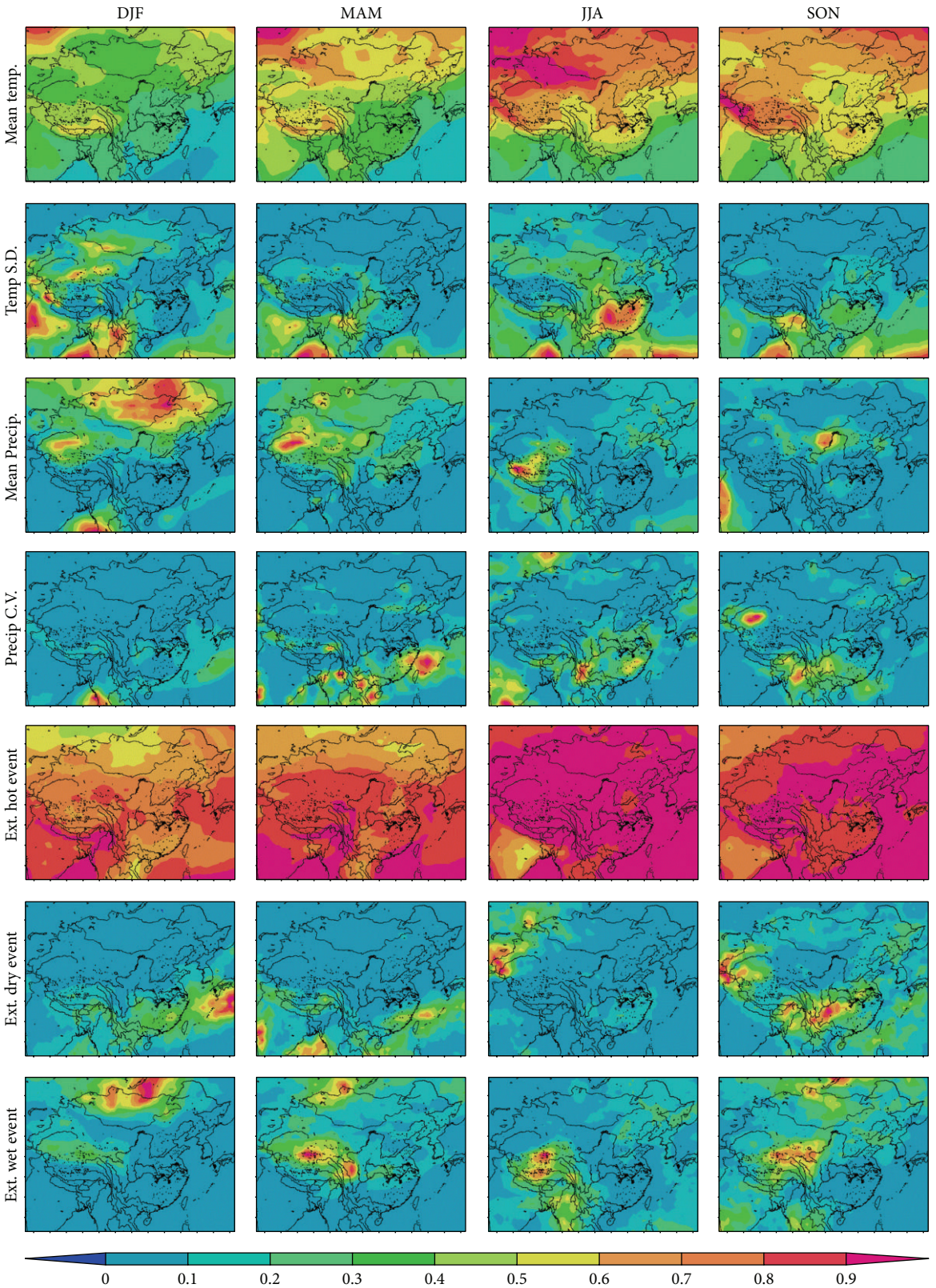

Figure 4: The absolute value of change which normalized to the maximum absolute value of all grid points in each variable between the period from 1970 to 1999 and the period from 2070 to 2099.

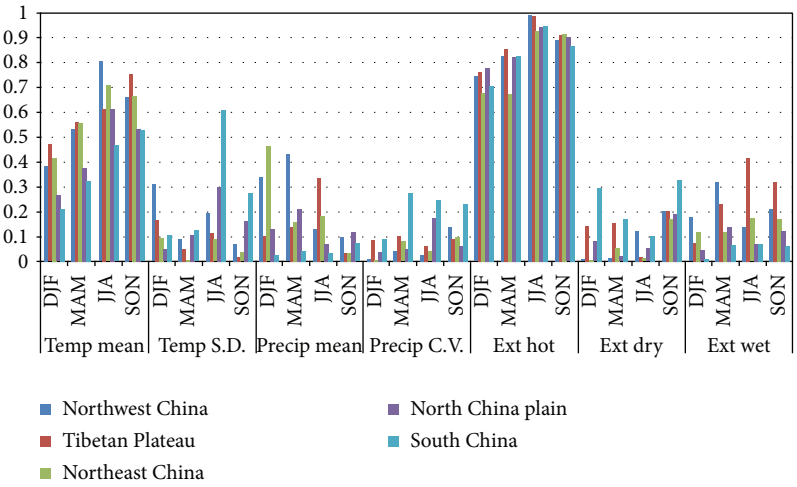

Figure 5: The area average normalized absolute value of change of each variable in five subregions between the period from 1970 to 1999 and the period from 2070 to 2099.

precipitation variability during SON; extreme hot during MAM; and extreme wet during DJF and MAM.

For the quantitative evaluation of the contribution from each variable to the relative aggregate climate change, the absolute value of change normalized to the maximum absolute value in the period from 2070 to 2099 (Figure 4). The change and the normalized change of variable share similar spatial distribution, which facilitates their comparison with other variables in terms of relative aggregate climate change contribution. Mean temperature and extreme hot event contributed more to aggregate climate change especially during JJA and SON than the other variables. The regions where mean precipitation increases significantly, like Tarim Basin and south Tibetan Plateau, exhibit a large contribution to SED and lead to a large extreme wet index. In contrast, the region precipitation decreases, like in South China, having a large extreme dry index especially during SON.

Figure 5 shows the normalized absolute change of each variable in different subregions. The extreme hot event has the greatest contribution to the hotspot identification index (greater than 0.7 and greater than 0.9 during JJA) of all subregions and with minimal spatial difference. The mean temperature has the second greatest contribution, especially during JJA and SON, in Northwest China, Tibetan Plateau, and Northeast China. The other variables have relatively small contributions to hotspot identification but with obvious spatial differences. Northwest China and Tibetan Plateau are identified as hotspots by other variables, such as mean precipitation, extreme wet event, and temperature variability. Northeast China exhibits the most obvious increase in mean precipitation during DJF. South China exhibits the most obvious changes in temperature and precipitation variability and extreme dry event, and North China Plain exhibits minimum changes as compared to other regions.

4. Conclusions and Discussion

Based on the CMIP5 projection, the seasonal temperature in most parts of China will increase more than 3°C, especially more than 4°C increase during MAM and JJA by the end of 21st century. The mean precipitation will increase in North China but will decrease in South China, especially during DJF and SON. The future increase in temperature and change in precipitation will also induce extreme climate events that can significantly affect human welfare and the environment especially in the countries vulnerable to the adverse impact of climate change, such as China. Therefore, the changes in the mean and extreme climates must be aggregated to identify the climate change hotspots in China within a special global warming target [38].

This paper applies SED to analyze the climate change signal over China from the CMIP5 ensemble. The relative aggregate climate change index includes several variables, such as the seasonal mean temperature and precipitation and their variability, extreme hot event, extreme dry event, and extreme wet event. SED increases over time and across different scenarios depending on the GHG emissions and concentrations. Our statistical metric of multidimensional climate change identifies Northwest China and Tibetan Plateau as two regional climate change hotspots in both the RCP4.5 and RCP8.5 forcing pathways. Our results are consistent with those from Xu et al. [25]. North China Plain exhibits a relatively small aggregate change to global warming, which is inconsistent with the results of Xu et al. [25]. Xu et al. [25] calculated the RCCI based on four variables (changes in mean temperature and precipitation as well as their variability) for two seasons (JJA and DJF). However, the variables and seasons that they employed in their calculations were different from those that we used in our analysis. For example, we project an increase and a decrease in the mean precipitation in North China during DJF and SON, respectively, but other studies may yield different projections by choosing different seasons.

Each climate variable offers different contributions to the relative aggregate climate change index. The extreme hot event and mean temperature are the two largest contributors to hotspot identification index over all subregions and with minimal spatial difference, which is consistent with the findings of Diffenbaugh and Giorgi [37]. In contrast, Diffenbaugh et al. [19] found that the hotspot pattern in the USA was shaped by the changes in the interannual variability more than by the changes in the long-term mean of the contributing variables. Such inconsistency is partly attributed to the differences in the variables, study area, and different methodologies of these studies. Given that we consider both the mean and extreme climate variables in our SED, we are able to evaluate the importance of extreme climate events in the identification of climate change hotspots.

The SED combines information from different indicators without weighting the importance of each indicator on the local climate change impacts. The adoption of different climate model data, subregion division, multidecadal scales, hotspots identification method, and variables may generate different measures of change. In addition, non-hotspot areas must not be considered as immune to climate change because such phenomenon can still exert a substantial impact on these areas. South China is identified as a climate change hotspot based on the change of extreme dry event during SON and DJF. However, this region has not been identified as a climate change hotspot based on the aggregate climate change index SED. The extreme drought events have been observed in South China [39–41] and are expected to become more frequent by the end of the century.

The SED is limited to represent the bidirectional change of the hotspots, and thus a strong increase in precipitation, which can be regarded as positive in some regions, may be perceived equally problematic as a strong decrease in precipitation. But it is still useful to identify the regions that are responsive and possibly vulnerable to climate change. Our hotspot analysis may significantly contribute to climate impact assessment, detection, and attribution as well as to the designing of national and cross-national adaptation and mitigation policies.

Conflict of Interests

The authors declare that there is no conflict of interests regarding the publication of this paper.

Acknowledgments

This work was supported by the National Basic Research Program of China (2010CB951101), China Postdoctoral Science Foundation funded Project (no. 2013M541598), the program of Dual Innovative Talents Plan and Innovative Research Team in Jiangsu Province, National Natural Science Foundation of China (no. 41323001, 41101015, and 41101016), and the Fundamental Research Funds for the Central Universities. The authors acknowledge the World Climate Research Programme's Working Group on Coupled Model, which is responsible for CMIP, and thank the climate modeling groups for producing and making available their model output.

References

[1] Contribution of Working Group I to the Fourth Assessment Report of the Intergovernmental Panel on Climate Change, "Climate change 2007: the physical basis," IPCC 4th Assessment Report (AR4), Cambridge University Press, New York, NY, USA, 2007.

[2] T. R. Karl and K. E. Trenberth, "Modern global climate change," *Science*, vol. 302, no. 5651, pp. 1719–1723, 2003.

[3] J. A. Patz, D. Campbell-Lendrum, T. Holloway, and J. A. Foley, "Impact of regional climate change on human health," *Nature*, vol. 438, no. 7066, pp. 310–317, 2005.

[4] G. Wang, "Agricultural drought in a future climate: results from 15 global climate models participating in the IPCC 4th assessment," *Climate Dynamics*, vol. 25, no. 7-8, pp. 739–753, 2005.

[5] T. P. Barnett, J. C. Adam, and D. P. Lettenmaier, "Potential impacts of a warming climate on water availability in snow-dominated regions," *Nature*, vol. 438, no. 7066, pp. 303–309, 2005.

[6] J. Sheffield and E. F. Wood, "Projected changes in drought occurrence under future global warming from multi-model, multi-scenario, IPCC AR4 simulations," *Climate Dynamics*, vol. 31, no. 1, pp. 79–105, 2008.

[7] Q. Schiermeier, "Increased flood risk linked to global warming," *Nature*, vol. 470, article 316, 2011.

[8] H. Gu, G. Wang, Z. Yu, and R. Mei, "Assessing future climate changes and extreme indicators in East and South Asia using the RegCM4 regional climate model," *Climatic Change*, vol. 114, no. 2, pp. 301–317, 2012.

[9] T. D. Mitchell and M. Hulme, "Predicting regional climate change: living with uncertainty," *Progress in Physical Geography*, vol. 23, no. 1, pp. 57–78, 1999.

[10] F. Giorgi and R. Francisco, "Evaluating uncertainties in the prediction of regional climate change," *Geophysical Research Letters*, vol. 27, no. 9, pp. 1295–1298, 2000.

[11] X. Gao, Y. Shi, D. Zhang, and F. Giorgi, "Climate change in China in the 21st century as simulated by a high resolution regional climate model," *Chinese Science Bulletin*, vol. 57, no. 10, pp. 1188–1195, 2012.

[12] T. Zhou and R. Yu, "Twentieth-century surface air temperature over China and the globe simulated by coupled climate models," *Journal of Climate*, vol. 19, no. 22, pp. 5843–5858, 2006.

[13] P. Zhai, A. Sun, F. Ren, X. Liu, B. Gao, and Q. Zhang, "Changes of climate extremes in China," *Climatic Change*, vol. 42, no. 1, pp. 203–218, 1999.

[14] P. Zhai, X. Zhang, H. Wan, and X. Pan, "Trends in total precipitation and frequency of daily precipitation extremes over China," *Journal of Climate*, vol. 18, no. 7, pp. 1096–1107, 2005.

[15] R. Yu and T. Zhou, "Seasonality and three-dimensional structure of interdecadal change in the East Asian monsoon," *Journal of Climate*, vol. 20, no. 21, pp. 5344–5355, 2007.

[16] Y. Qiu, W. Cai, X. Guo, and A. Pan, "Dynamics of late spring rainfall reduction in recent decades over Southeastern China," *Journal of Climate*, vol. 22, no. 8, pp. 2240–2247, 2009.

[17] R. Wu, Z. Wen, S. Yang, and Y. Li, "An interdecadal change in southern China summer rainfall around 1992/93," *Journal of Climate*, vol. 23, no. 9, pp. 2389–2403, 2010.

[18] T. Zhou, D. Gong, J. Li, and B. Li, "Detecting and understanding the multi-decadal variability of the East Asian Summer Monsoon—recent progress and state of affairs," *Meteorologische Zeitschrift*, vol. 18, no. 4, pp. 455–467, 2009.

[19] N. S. Diffenbaugh, F. Giorgi, and J. S. Pal, "Climate change hotspots in the United States," *Geophysical Research Letters*, vol. 35, no. 16, Article ID L16709, 2008.

[20] A. de Sherbinin, "Climate change hotspots mapping: what have we learned?" *Climatic Change*, vol. 123, no. 1, pp. 23–37, 2014.

[21] F. Giorgi, "Climate change hot-spots," *Geophysical Research Letters*, vol. 33, no. 8, Article ID L08707, 2006.

[22] N. S. Diffenbaugh, M. Ashfaq, B. Shuman, J. W. Williams, and P. J. Bartlein, "Summer aridity in the United States: response to mid-holocene changes in insolation and sea surface temperature," *Geophysical Research Letters*, vol. 33, no. 22, Article ID L22712, 2006.

[23] M. B. Baettig, M. Wild, and D. M. Imboden, "A climate change index: where climate change may be most prominent in the 21st century," *Geophysical Research Letters*, vol. 34, no. 1, Article ID L01705, 2007.

[24] J. W. Williams, S. T. Jackson, and J. E. Kutzbach, "Projected distributions of novel and disappearing climates by 2100 AD," *Proceedings of the National Academy of Sciences of the United States of America*, vol. 104, no. 14, pp. 5738–5742, 2007.

[25] Y. Xu, X. Gao, and F. Giorgi, "Regional variability of climate change hot-spots in East Asia," *Advances in Atmospheric Sciences*, vol. 26, no. 4, pp. 783–792, 2009.

[26] D. Jiang and Z. Tian, "East Asian monsoon change for the 21st century: results of CMIP3 and CMIP5 models," *Chinese Science Bulletin*, vol. 58, no. 12, pp. 1427–1435, 2013.

[27] J. Zhang, L. Li, T. Zhou, and X. Xin, "Evaluation of spring persistent rainfall over East Asia in CMIP3/CMIP5 AGCM simulations," *Advances in Atmospheric Sciences*, vol. 30, no. 6, pp. 1587–1600, 2013.

[28] Y. Yao, Y. Luo, J. Huang, and Z. Zhao, "Comparison of monthly temperature extremes simulated by CMIP3 and CMIP5 models," *Journal of Climate*, vol. 26, pp. 7692–7707, 2013.

[29] H. Ju, M. Velde, E. Lin, W. Xiong, and Y. Li, "The impacts of climate change on agricultural production systems in China," *Climatic Change*, vol. 120, pp. 313–324, 2013.

[30] Y. Lin, A. Liu, E. Ma, and F. Zhang, "Impacts of future climate changes on shifting patterns of the agro-ecological zones in China," *Advances in Meteorology*, vol. 2013, Article ID 163248, 9 pages, 2013.

[31] C. L. Weber, G. P. Peters, D. Guan, and K. Hubacek, "The contribution of Chinese exports to climate change," *Energy Policy*, vol. 36, no. 9, pp. 3572–3577, 2008.

[32] J. S. Gregg, R. J. Andres, and G. Marland, "China: emissions pattern of the world leader in CO_2 emissions from fossil fuel consumption and cement production," *Geophysical Research Letters*, vol. 35, no. 8, Article ID L08806, 2008.

[33] Y. Guo, W. J. Dong, F. M. Ren, Z. C. Zhao, and J. B. Huang, "Assessment of CMIP5 simulations for China annual average surface temperature and its comparison with CMIP3 simulations," *Advances in Climate Change Research*, vol. 9, pp. 181–186, 2013.

[34] Y. Xu and C. Xu, "Preliminary assessment of simulations of climate changes over China by CMIP5 multi-models," *Atmospheric and Oceanic Science Letters*, vol. 5, no. 6, pp. 489–494, 2012.

[35] R. H. Moss, J. A. Edmonds, K. A. Hibbard et al., "The next generation of scenarios for climate change research and assessment," *Nature*, vol. 463, no. 7282, pp. 747–756, 2010.

[36] J. Rogelj, M. Meinshausen, and R. Knutti, "Global warming under old and new scenarios using IPCC climate sensitivity range estimates," *Nature Climate Change*, vol. 2, no. 4, pp. 248–253, 2012.

[37] N. Diffenbaugh and F. Giorgi, "Climate change hotspots in the CMIP5 global climate model ensemble," *Climatic Change*, vol. 114, pp. 813–822, 2012.

[38] A. Kitoh, H. Endo, K. Krishna Kumar, I. F. A. Cavalcanti, P. Goswami, and T. Zhou, "Monsoons in a changing world: a regional perspective in a global context," *Journal of Geophysical Research: Atmospheres*, vol. 118, pp. 3053–3065, 2013.

[39] Z.-Z. Hu, S. Yang, and R. Wu, "Long-term climate variations in China and global warming signals," *Journal of Geophysical Research D: Atmospheres*, vol. 108, no. 19, 2003.

[40] X. Xin, R. Yu, T. Zhou, and B. Wang, "Drought in late Spring of South China in recent decades," *Journal of Climate*, vol. 19, no. 13, pp. 3197–3206, 2006.

[41] D. Jin, Z. Guan, and W. Tang, "The extreme drought event during Winter–Spring of 2011 in East China: combined influences of teleconnection in midhigh latitudes and thermal forcing in maritime continent region," *Journal of Climate*, vol. 26, pp. 8210–8222, 2013.